Eur Biophys J (2010) 39:1375–1384
DOI 10.1007/s00249-010-0591-1

ORIGINAL PAPER

Comparing native and irradiated *E. coli* lactose repressor-operator complex by molecular dynamics simulation

Samia Aci-Sèche · Norbert Garnier · Stéphane Goffinont · Daniel Genest · Mélanie Spotheim-Maurizot · Monique Genest

Received: 17 December 2009 / Revised: 22 February 2010 / Accepted: 28 February 2010 / Published online: 28 March 2010

Abstract The function of the *E. coli* lactose operon requires the binding of the tetrameric repressor protein to the operator DNA. We have previously shown that γ-irradiation destabilises the repressor-operator complex because the repressor gradually loses its DNA-binding ability (Radiat Res 170:604–612, 2008). It was suggested that the observed oxidation of tyrosine residues and the concomitant structural changes of irradiated headpieces (DNA-binding domains of repressor monomers) could be responsible for the inactivation. To unravel the mechanisms that lead to repressor-operator complex destabilisation when tyrosine oxidation occurs, we have compared by molecular dynamic simulations two complexes: (1) the native complex formed by two headpieces and the operator DNA, and (2) the damaged complex, in which all tyrosines are replaced by their oxidation product 3,4-dihydroxyphenylalanine (DOPA). On a 20 ns time scale, MD results show effects consistent with complex destabilisation: increased flexibility, increased DNA bending, modification of the hydrogen bond network, and decrease of the positive electrostatic potential at the protein surface and of the global energy of DNA-protein interactions.

Keywords Ionising radiation · Protein oxidation · DNA-protein complex · Molecular dynamics

S. Aci-Sèche · N. Garnier · S. Goffinont · D. Genest · M. Spotheim-Maurizot · M. Genest (✉)
Centre de Biophysique Moléculaire, UPR 4301, CNRS (affiliated to the University of Orléans and to INSERM), rue Charles Sadron, 45071 Orléans Cedex 02, France
e-mail: m.genest@cnrs-orleans.fr

N. Garnier
University of Orléans, rue Charles Sadron, 45071 Orléans Cedex 02, France

Introduction

The regulation of the expression of genes involved in the *E. coli* metabolism of lactose operon requires the binding of a protein, the repressor, to a specific DNA sequence, the operator (Wilson et al. 2007). The lactose repressor is a homotetrameric protein organised as a dimer of dimers. It contains a tetrameric core (formed by the C-terminal regions of the four monomers) and four DNA-binding domains called headpieces (each one being the N-terminal region of a monomer), linked to the core by a hinge. The two dimers are assembled via a 4-helix bundle called tetramerisation domain (formed by the final C-terminal helices of each core monomer). The two monomers of a dimer are held together by strong interactions between their core regions. The free headpiece contains three α helices linked by loops. The hinge region is unfolded in a free state and folds into a helix upon binding to DNA.

The first two helices form, together with their connecting loop, the helix-turn-helix (HTH) motif which directly interacts with the major groove of operator DNA. The second helix is called the recognition helix. Formation of the repressor-operator complex requires the binding of at least one headpiece pair (via the two headpieces of the same dimer) to the operator (Kalodimos et al. 2004; Spronk et al. 1996).

We have previously shown that upon irradiation with γ rays the repressor-operator complex is destabilised mainly because the repressor losses its DNA binding ability (Eon et al. 2001).

Retardation gel electrophoresis experiments have shown that the amount of complex between the tetrameric repressor and the DNA decreases with increasing irradiation dose and that a new complex between DNA and a dimeric repressor still able to bind DNA is produced. The dimeric

repressor is formed by the splitting of the tetramer in two dimers due probably to the damage of the tetramerisation domain. By further increasing radiation doses this complex is also destabilised (Goffinont et al. 2009). It is most probable that the loss of binding ability of both the tetrameric and the dimeric repressors is at least partially due to the damage of the headpieces. Therefore, and because of calculation limitations, we have chosen to study by molecular dynamics simulation the effect of headpiece radiation-induced modifications on the stability of the DNA-headpiece pair system. However, besides the modification of the oligomerisation state of the protein, damage to the core can also affect the binding of the headpieces to DNA by an allosteric effect. It is known that binding of IPTG to the core of the lactose repressor hinders its binding to DNA by inducing a global structural change including the modification of the positioning of the HPs (Wilson et al. 2007).

By mass spectrometry the most frequent lesions of headpieces irradiated free in solution (in absence of DNA) have already been identified; all tyrosine residues are modified into their oxidation product (Jain et al. 1997), 3, 4-dihydroxyphenylalanine (DOPA; Gillard et al. 2007). Tyrosines are the most reactive and accessible amino acids of the headpiece also according to calculations with the model RADACK (Begusova et al. 2001). Spectroscopic measurements and molecular dynamics simulation have revealed that tyrosine oxidation can induce changes in the structure and the stability of a free headpiece (Mazier et al. 2008).

To understand how headpiece damage can contribute to the observed radiation-induced destabilisation of the operator-repressor complex, it is necessary to consider the consequences of the protein damage on the structural properties of the entire headpiece-operator complex with special attention to the different types of interactions (electrostatic, hydrophobic, etc.) between the partners. Therefore we have studied and compared two complexes using molecular dynamics simulations: (1) the native complex formed by a pair of headpieces and a fragment of DNA duplex with the operator sequence and (2) the damaged complex in which all tyrosine residues of the headpieces are replaced by DOPA (see Fig. 1). Based on an NMR-based structure of the native complex deposited at the Protein Data Bank (PDB ID: 1CJG; Berman et al. 2000; Spronk et al. 1999), 20 ns trajectories were produced for each complex and the consequences for the structure, the flexibility and the interactions of the different partners in the complexes were analysed. However, it was not expected that the separation of the headpiece molecules from the operator could be monitored within such a short time.

Simplified models such as those based on implicit solvent coarse-graining can be used to access longer time simulations (Klepeis et al. 2009). However, these techniques are not as predictive as all-atom simulations which are particularly well suited to study subtle conformational changes that may have strong impact, despite their small magnitude. Thus, the atomistic approach is used in this work with the aim to have a detailed view of the primary events that may trigger the separation of headpiece molecules from the operator.

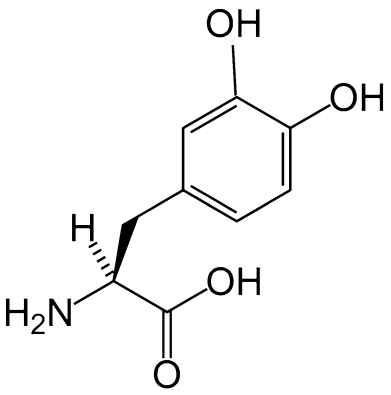

Fig. 1 Dihydroxyphenylalanine (DOPA)

Materials and methods

Initial structures

The headpiece structure (PDB ID: 1CJG) determined by NMR spectroscopy (Spronk et al. 1999) was used as initial structure for building the complex including the self complementary 22 bp operator DNA and two 62 amino acid free identical headpieces (see Table 1 for sequences). The damaged complex was obtained by replacing each of the 4 tyrosines of the native protein by their oxidation product DOPA. DOPA parameters were created using the Antechamber program of the AMBER package (Case et al. 2002). Atomic charges and atom names are given in Table 2.

The protein sequences were terminated by N-terminal (CH3-CO) and C-terminal (CHCH3) end groups, and 38 Na^+ counter ions were added to neutralise the complexes. Each complex with its counter ions was centred in a truncated octahedron box of TIP3P water molecules.

The final number of atoms was 55,123 and 55,083 for the native and the damaged complexes respectively.

Molecular dynamics (MD) simulation procedure

Ten thousands steps of energy minimisation were first performed to remove possible wrong interatomic contacts in the initial structure. Then the systems were heated in the NVT ensemble from 0 to 300 K by steps of 50 K. During

Table 1 Repressor headpiece amino acid sequence and DNA base sequence of the native complex (PDB ID:1CJG)

Tyr residues are in *bold* and replaced with DOPA in the damaged complex. The four α-helices of the headpiece are *underlined*

Sequences
Headpiece aa sequence
MET_1 LYS PRO VAL THR LEU **TYR** ASP VAL ALA GLU **TYR** ALA GLY VAL
SER_{16} **TYR** GLN THR VAL SER ARG VAL VAL ASN GLN ALA SER HIS VAL
SER_{31} ALA LYS THR ARG GLU LYS VAL GLU ALA ALA MET ALA GLU LEU
ASN_{46} **TYR** ILE PRO ASN ARG VAL ALA GLN GLN LEU ALA GLY LYS GLN
SER_{61} LEU
DNA base sequence
5′-G_1 A A T T G T G A G_{10} C G C T C A C A A T_{20} T C -3′
3′-C T T_{20} A A C A C T C G C G_{10} A G T G T T A A G_1 -5′

Table 2 Atomic charges on tyrosine and DOPA

Tyrosine		DOPA	
Atom	Charges	Atom	Charges
N	−0.4157	N	−0.4157
H	0.2719	H	0.2719
CA	−0.0014	CA	−0.0014
HA	0.0876	HA	0.0876
CB	−0.0152	CB	−0.0224
HB2	0.0295	HB2	0.0732
HB3	0.0295	HB3	0.0732
CG	−0.0011	CG	−0.0767
CD1	−0.1906	CD1	−0.1292
HD1	0.1699	HD1	0.1356
CE1	−0.2341	CE1	−0.1682
HE1	0.1656	HE1	0.1343
CZ	0.3226	CZ	0.0373
OH	−0.5579	OH	−0.5182
HH	0.3992	HH	0.4279
CE2	−0.2341	CE2	0.1079
		OH2	−0.5013
HE2	0.1656	HH2	0.4365
CD2	−0.1906	CD2	−0.1366
HD2	0.1699	HD2	0.1549
C	0.5973	C	0.5973
O	−0.5679	O	−0.5679

this process the position of the atoms of the protein and of the DNA was constrained with a harmonic potential in order to avoid distortion of the solute structure. This was followed by an MD run at 300 K in the same ensemble with a progressive decrease of the constraints on the solute atoms until their complete removal. Then an MD run at 300 K in the NPT ensemble was performed to equilibrate the systems until density stability. This last step was 1.5 ns for the native and 4 ns for the damaged complex. The last conformation of the equilibration state was taken as starting structure for producing a 20 ns MD trajectory for each complex in the NPT ensemble at 300 K. Snapshots were stored every 10 ps giving finally a collection of 2,000 conformations. In all MD runs, the SHAKE (Ryckaert et al. 1977) algorithm was used to maintain a constant length of the covalent bonds involving a hydrogen atom. Electrostatic forces were computed with the Particle Mesh Ewald (PME) method (Darden et al. 1993). All simulations were performed with the AMBER9 package (Case et al. 2002).

Analysis of MD trajectories

RMSD

The root mean square deviation (RMSD) between two structures of a molecular system allows their differences to be quantified. It is computed as $\text{RMSD} = [(1/N_a) \times \Sigma(r_{i1} - r_{i2})^2]^{1/2}$ in which N_a is the number of atoms and r_{i1} and r_{i2} are the position vectors i in the first and second structures respectively. The sum runs from $i = 1$ to $i = N_a$. The molecular system can be a group of atoms or molecules, a unique molecule or part of a molecule. Computing the RMSD necessitates the removal of the overall motions of the molecular systems.

In our study, when the RMSD between a structure of the native complex and a structure of the damaged complex is computed, only backbone atoms N, Cα, C, O, and P are considered. When RMSD between two conformations of the same complex (native or damaged) is computed, all heavy atoms are used.

Most central structure

Averaging each atom position in a collection of conformations of a flexible molecular system describes a mean structure which is generally not a realistic one. In this work we consider the most central structure of the collection instead of the mean structure. It is defined as the conformation k such that $\Sigma(\text{RMSD}_{kl})^2$ is minimum, RMSD_{kl} being the RMSD between conformations k and l, and the sum runs over all the conformations $l \neq k$ of the collection. In the

following, the most central conformation will be termed central structure.

Flexibility 2D map

An interesting descriptor of the flexibility of a molecular system is the amplitude of the fluctuations of interatomic distances. Indeed, if all the distances between a set of atoms are constant over a collection of conformations, this means that the atoms behave as a rigid body. If the distances fluctuate, they are characteristic of a deformable body. The mean amplitude of fluctuations of the distances between two atoms i and j is given by: $\langle \delta_{ij} \rangle = [(1/N_c) \sum (d_{ij}(c) - \langle d_{ij} \rangle)^2]^{1/2}$ where N_c is the number of conformations ($N_c = 2{,}000$ in this study) and $d_{ij}(c)$ and $\langle d_{ij} \rangle$ are the distances between atoms i and j calculated in conformation c and in the mean structure respectively. The sum extends over all conformations ($c = 1$ to N_c).

A 2D graphic representation of all the $\langle \delta_{ij} \rangle$ allows an easy visualisation of the regions of the molecular systems that are quasi-rigid and those that are more flexible.

DNA structure

The different conformational parameters of DNA were analysed for the central structure of each complex using the program CURVES (Lavery and Sklenar 1988). Time series of the DNA curvature was further refined with MADBEND (Strahs and Schlick 2000). For this analysis, the two base pairs at each extremity of the DNA sequence were excluded.

Hydrogen bonds

Hydrogen bonds (HB) analysis was performed on the whole trajectories with the program CARNAL of the AMBER7 package. An HB is assumed to be present when the distance between the donor (D) and the acceptor (A) is smaller than 3.5 Å and the angle D–H–A is between 120° and 180°. Only HBs that are present in more than 50% of the 2,000 stored conformations are considered.

Binding free energy calculations

Binding free energies were calculated following the MM-PB(GB)SA approach (Kollman et al. 2000; Srinivasan et al. 1998) according to $\Delta G_{\text{binding}} = \langle G^{\text{complex}}(i) \rangle_i - \langle G^{\text{protein}}(i) \rangle_i - \langle G^{\text{DNA}}(i) \rangle_I$ where $\langle \ldots \rangle$ denotes an average over snapshots i taken from MD trajectories and $G^x(i)$ was estimated from contributions of gas phase energies and solvation free energies:

$$G^x(i) = \mathrm{H}^x_{\text{gas}}(i) + G^x_{\text{solvation}}(i).$$

H_{gas} of the solute were calculated by summing contributions from internal energies (including coulombic energy, van der Waals energy as determined by a Lennard-Jones potential and internal energy). $G^x_{\text{solvation}}$ was calculated as the sum of polar and nonpolar contributions. The polar contribution was calculated with the Generalized Born (GB) model as implemented in AMBER 9.

Electrostatic potential

Electrostatic potential at the surface of the pair of headpieces was calculated using APBS program (Baker et al. 2001; Dolinsky et al. 2004, 2007), and the graphic representation was performed with Chimera (Pettersen et al. 2004).

Results

RMSD

The two central structures which represent respectively the native and the damaged complexes do not present large differences in their backbones (Fig. 2). They are separated by an RMSD value of only 1.5 Å whereas they are separated by an RMSD smaller than 3 Å with respect to the experimental structure. This shows that none of the complexes has diverged drastically from the experimental structure during the 20 ns simulations. In particular the secondary structure of the headpiece is fully conserved in both simulations.

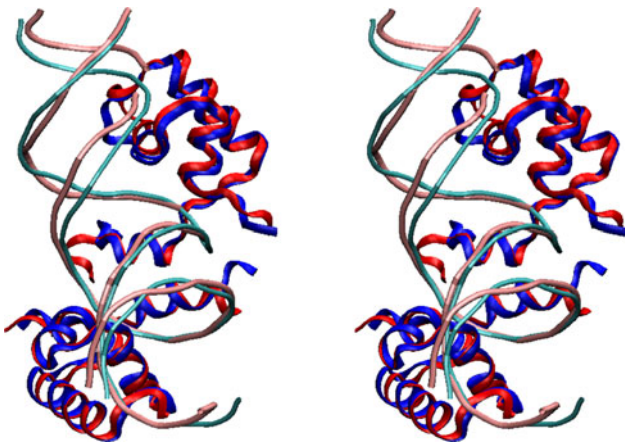

Fig. 2 Stereo view of the most central structures of damaged (*red* and *pink*) and native (*blue* and *cyan*) complexes. Alignment was performed on N, Cα, C, O and P atoms. The pair of headpieces is represented with *ribbons* and DNA duplexes with *tubes*. Visualisation with VMD (Humphrey et al. 1996)

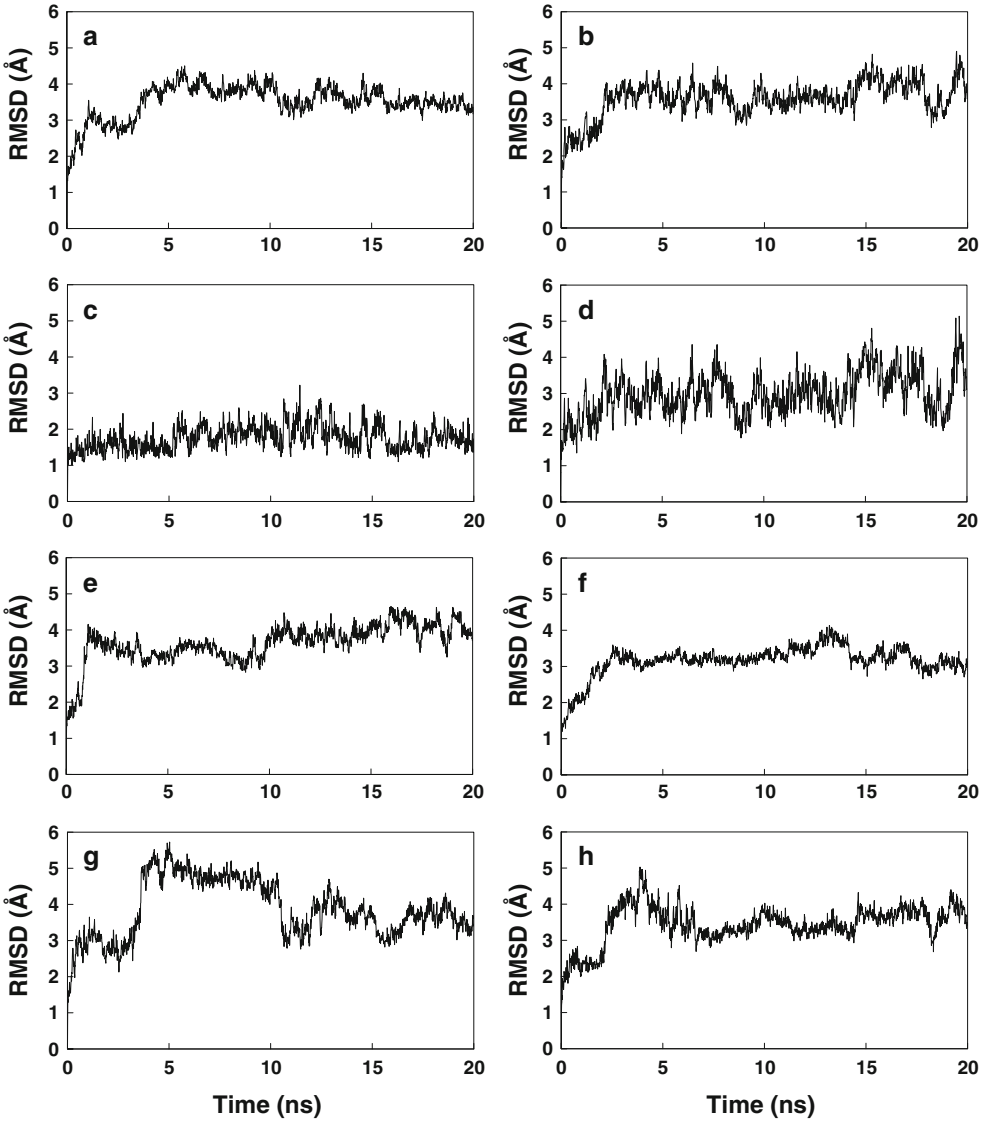

Fig. 3a–h RMSD evolution during the 20 ns simulations of native (*left*) and damaged (*right*) complexes. **a**, **b** Whole complex; **c**, **d** DNA; **e**, **f** monomer 1; **g**, **h** monomer 2. RMSD is calculated over all heavy atoms

Figure 3a, b shows the evolution of the RMSD of both complexes relative to the first conformation of their production period. Although both curves exhibit approximately the same mean value, the fluctuations in the damaged complex are larger indicating an increased internal dynamics. In order to get more insight about this observation, the RMSD evolution of each component of the ternary complexes was examined. For the protein molecules (Fig. 3e–h), no clear conclusions can be drawn as the RMSD of each headpiece evidences several transitions between metastable conformations.

The most drastic difference in the RMSD evolution concerns the DNA duplex (Fig. 3c, d). Indeed average values are 1.8 and 3.0 Å in the native and the damaged complexes respectively. In addition structural fluctuations are much larger when tyrosines are replaced by DOPA. The difference in average RMSD is probably the result of a deformation of the DNA in the early stage of the simulation. But the increase in RMSD fluctuations evidences a partial loss of interactions between DNA and the headpieces.

Internal flexibility

Figure 4 shows 2D maps representing the average amplitude of the fluctuations of each interatomic distance during the simulations, giving a direct representation of the internal flexibility of the complexes. It is clearly shown that all the regions of the map corresponding to the damaged complex (Fig. 4b) present a larger internal dynamics of the complex. On average, interatomic distance fluctuations are much larger than in the native complex by 46%. However, the dynamics increase is not equally spread over the different regions of the complex. It ranges between 25% for atom pairs belonging to DNA and 75% for atom pairs belonging to monomer 2. Largest increases are observed

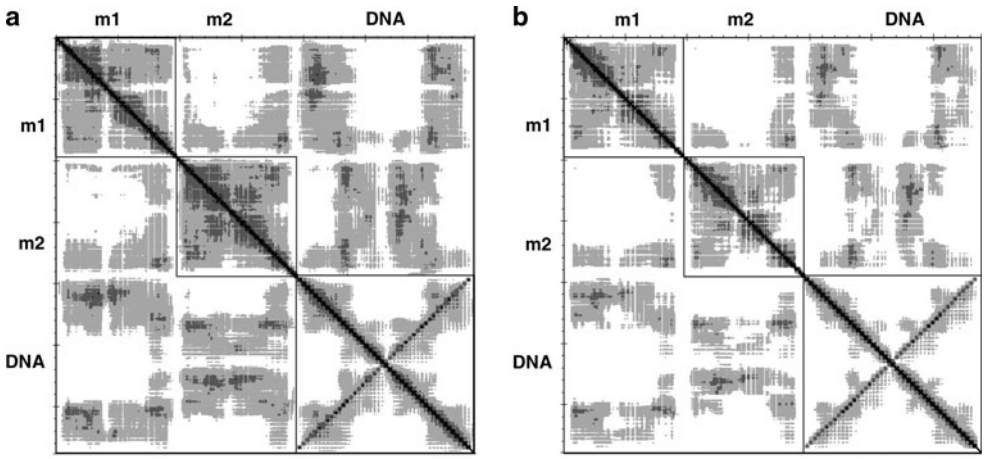

Fig. 4 Internal flexibility of the native (**a**) and damaged complexes (**b**). Frames correspond to the intramolecular flexibility of the different partners (m1, m2, DNA) of the complexes. The 2D maps represent the amplitude of the interatomic distance fluctuations averaged over the whole simulation time. Each point is colored according to the average value: *black* <0.1 Å; *dark grey* between 0.1 and 0.25 Å; *light grey* between 0.25 and 0.50 Å; *white* >0.50 Å. Each dimension of the maps represents the atom numbers

for distances involving at least one atom of the second headpiece monomer.

This analysis demonstrates a decrease in interactions between the two headpieces and the DNA fragment of the DOPA complex.

Intermolecular hydrogen bonds

Hydrogen bonds are not detected at a significant level between both headpiece monomers during the simulations. On the contrary, many intermolecular HBs involving DNA and the monomers are observed, some of them being very stable while others are rather labile. In the case of the native complex, 35 of these intermolecular HBs are observed during more than 50% of the simulation time while only 31 are detected more than 50% of the time in the damaged complex. If we consider the most stable HBs as those present more than 75% of the simulation time, the difference in hydrogen-bonded interactions between both complexes is even more evident (30 HBs for the native complex compared to 22 for the damaged complex).

More precisely, at the level of the recognition helices (helix 2) which are in contact with DNA, hydrogen bond interactions are much weaker in the damaged complex. In the native complex nine residues located on helix 2 are linked to a nucleotide for more than 75% of the simulation time, while in the damaged complex only five residues belonging to helix 2 are involved in strong hydrogen-bonded interaction with DNA.

Table 3 gives an overview of the amino acids linked to a nucleotide by at least one H-bond for more than 50% of the simulation time. The results clearly evidence a loss of stability of the damaged complex.

During the simulations, DNA is observed as proton donor for a few HBs, involving three symmetrical pairs, G12, C13 and C15, of each DNA strand and Ala53, Tyr7/DOPA7 and Gln18 of the headpiece monomers.

Two of these pairs [N_4H_{42} (C13) → OH(Tyr7) and N_4H_{42} (C15) → OH(Gln18)] are already present in the experimental structure. However, during the simulation of the damaged complex the C13-DOPA7 HB established in monomer 2 is unstable and disappears after a few nanoseconds and the C15-Gln18 HB in the same monomer 2 is formed less than 50% of the time.

For most of the intermolecular HBs, DNA is proton acceptor. As observed in the experimental structure, 13 of this HB type are present which implies residues Leu6, Tyr12, Tyr47 and Asn50 with the C13 nucleotide, Gln54 with T14, Lys59 with C11 and Ser 61 with C15. Along the trajectories, the Tyr12/DOPA12-C13 interaction is observed less than 25% of the time. HBs involving residues Lys59 and Ser61 are very labile as they establish successive weak interactions with different nucleotides. MD results are in agreement with the experiments since Ser61 in only one monomer is H-connected to C15 of one DNA strand. The other H-bonds observed in the NMR structure are strongly maintained all along the simulation.

Finally, several other transient intermolecular DNA-acceptor HBs appeared during the simulations, their stability being globally higher for the native complex (Table 3).

DNA structure

The analysis with CURVES of the central structures of DNA duplexes does not reveal major differences: helical

Table 3 Residues linked to nucleotides by at least one HB present at more than 50% of the simulation time in native and damaged complexes

Native (m1)	Native (m2)	Damaged (m1)	Damaged (m2)	Location
Leu6 → C13(s2)	Leu6 → C13(s1)	Leu6 → C13(s2)	Leu6 → C13(s1)	Helix 1
C13(s2) → Tyr7[a]	C13(s1) → Tyr7	C13(s2) → DOPA7	–	Helix 1
–	–	–	DOPA7 → T14(s1)[a]	Helix 1
Ser16 → G6(s1)	Ser16 → G6(s2)	Ser16 → G6(s1)	Ser16 → G6(s2)	
–	Tyr17 → G8(s2)	DOPA17 → G8(s1)	DOPA17 → G8(s2)	Helix 2
–	Gln18 → G6(s2)	–	–	Helix 2
C15(s2) → Gln18	C15(s1) → Gln18	C15(s2) → Gln18	–	Helix 2
Thr19 → G6(s1)	Thr19 → G6(s2)	Thr19 → G6(s1)	Thr19 → G6(s2)	Helix 2
Ser21 → T14(s2)	–	–	–	Helix 2
Arg22 → T5(s2)	–	–	–	Helix 2
–	Arg22 → G6(s2)	Arg22 → G6(s2)[a]	–	Helix 2
–	Asn25 → T14(s1)[a]	–	–	
His29 → T4(s1)[a]	–	–	–	
Val30 → T4(s1)	–	–	–	
Ser31 → T5(s1)	Ser31 → T5(s2)	Ser31 → T5(s1)	Ser31 → T5(s2)	
Thr34 → T5(s1)	Thr34 → T5(s2)	Thr34 → T5(s1)	Thr34 → T5(s2)	Helix 3
Tyr47 → C13(s2)	Tyr47 → C13(s1)	DOPA47 → C13(s2)	DOPA47 → C13(s1)	
Asn50 → C13(s2)	Asn50 → C13(s1)	Asn50 → C13(s2)	Asn50 → C13(s1)	
G12(s2) → Ala53	G12(s1) → Ala53[a]	G12(s2) → Ala53[a]	G12(s1) → Ala53[a]	Helix 4
Gln54 → T14(s2)	Gln54 → T14(s1)	Gln54 → T14(s2)	Gln54 → T14(s1)	Helix 4

Arrow goes from donor to acceptor. Headpiece monomers are named *m1* and *m2*, and DNA strands are named *s1* and *s2*. *Underlined* residues are also present in the experimental NMR structure (1CJG)

[a] HB present 50–75% of the simulation time

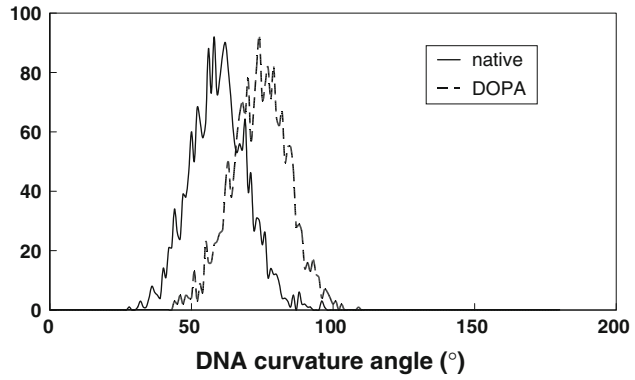

Fig. 5 Histograms of the curvature angle of the DNA axis calculated with MADBEND (Strahs and Schlick 2000) from the snapshots collected during the simulations of the native (*full line*) and the damaged (*dashed line*) complexes

and base orientation parameters of both complexes are similar. However, a slight increase of about 8° of the axis curvature is observed in the damaged complex while in the native complex DNA curvature remains very close to that observed in the experimental structure. A further refinement of DNA parameters with MADBEND reveals a mean increase of 14° of the axis curvature (from 59° to 73°) for the damaged complex (Fig. 5).

Binding free energy calculation

The different components of the free energy of both complexes have been evaluated under the frame of the Generalized Born (GB) approximation.

Binding free energy values were averaged over 2,000 snapshots taken at 10 ps intervals from the complete trajectories. Mean values of ΔGBTOT can be estimated to within a standard error of 14 and 11 kcal mol^{-1} in the case of the native and damaged complexes respectively (Table 4). Calculated binding free energies obtained with GB are −202 and −185 kcal mol^{-1} respectively. The free energy of the interaction between DNA and the headpiece pair is in favor of the native complex by 17 kcal mol^{-1}. This is mainly due to an increase in the electrostatic contribution of the DNA-protein interaction in the damaged complex which is not fully compensated by solvation effects. Therefore it is expected that the damaged headpieces should be less attracted by DNA than the native ones. An electrostatic effect is not surprising as the additional polar OH group in DOPA dramatically modifies the charge repartition in the aromatic ring (see Table 2).

A representation of the electrostatic potential at the surface of the headpiece pair given in Fig. 6 confirms this effect. Indeed it can be seen that the contacting surface of

Table 4 Binding free energy components of the headpiece complexes calculated from the 20 ns trajectories

Contribution[c]	ΔG binding[a], native complex		ΔG binding[a], damaged complex		Δ(ΔG binding)[b]	
	Mean[d]	σ[e]	Mean[d]	σ[e]	Contribution[c]	Mean[d]
ΔGAS	−4,300	±225	−4,146	±151	Δ(ΔGAS)	−154
ΔGBSOL	4,098	±219	3,961	±149	Δ(ΔGBSOL)	137
ΔGBELE	58	±13	88	±12	Δ(ΔGBELE)	−30
ΔGBTOT	−202	±14	−185	±11	Δ(ΔGBTOT)	−17

All values are in kcal mol^{-1}

[a] ΔG binding = contribution (complex) − contribution DNA − contribution headpiece pair

[b] Δ(ΔG binding) = ΔG binding native complex − ΔG binding damaged complex

[c] GAS = coulombic energy + van der Waals energy + internal energy (bond, angle, torsion); GBSOL = non polar free energy + polar solvation free energy in the GB model; GBELE = polar solvation free energy in the GB model + internal coulombic energy; GBTOT = GBSOL + GAS

[d] Average over 2,000 snapshots taken from the 20 ns trajectory

[e] Standard error

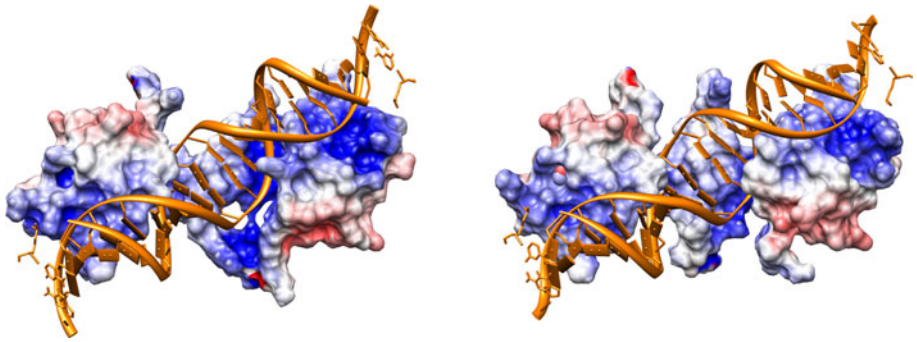

Fig. 6 View of the electrostatic potential at the surface of the pair of headpieces (from −5 to +5 V): native complex (*left*), damaged complex (*right*). Negative, positive and neutral potentials are coloured in *red*, *blue* and *white*, respectively

the headpieces with DNA is less positive in the damaged complex than in the native one (density of blue surface is smaller in the damaged complex).

Discussion and conclusion

The goal of the present study was to search the reasons for the destabilisation of the repressor-operator complex due to the loss of affinity of an irradiated repressor for the DNA operator. Our experiments have shown that the loss of affinity can be due at least partially to the damage of the headpieces (Goffinont et al. 2009). Therefore and because of calculation limitations related to the size of the entire repressors we have chosen to study only a part of the repressor-operator system, formed by two free headpieces and the DNA fragment. Different chemical modifications of the headpiece have been previously demonstrated, the most important one being the oxidation of tyrosine residues into DOPA. We have introduced in silico these modifications in the headpieces and followed their effects on the structure and stability of the complex. Molecular dynamics simulation including explicit representation of the solvent is a powerful technique for analysing structural, dynamic and energetic events at atomic resolution. Unfortunately it is time consuming and the explored time scale is limited to a few tens of nanoseconds, precluding the observation of large structural changes, such as the disruption of the modified complex or drastic conformational transitions into individual molecules of the complex. However, comparison between simulated trajectories of native and modified complexes is thought to bring about information on their relative stability.

A first observation is that the overall structure of both complexes is not submitted to modifications during the 20 ns trajectories, with the exception of a moderate increase in the DNA bending relative to the experimental structure in the damaged complex. A second observation is a significant increase in the internal dynamics in this last complex, indicative of a loss of stability of the structure. This is evidenced by increased fluctuations of interatomic distances and of RMSD, and is additionally explained by a reduced intermolecular hydrogen bond network and by a less negative binding energy. The cause of the weaker interaction between the headpiece pair and DNA in the damaged complex is mainly electrostatic. Therefore the atoms in this complex are less constrained and it seems reasonable to anticipate that their increased motions in the

nanosecond time scale, allowing a larger conformational exploration, could lead to much larger structural modification including molecule separation in the microsecond or millisecond time scales.

The observation that the atoms of monomer 2 are more mobile than those of monomer 1 in the simulation of the damaged complex reveals that the structure has not yet converged. This suggests that we are in the presence of primary events of a very slow transition (relative to the nanosecond range) which could lead to molecule dissociation as experimentally observed (Eon et al. 2001). Once the dissociation of the damaged complex is achieved, the headpiece monomers could undergo structural modifications such as loss of helicity already reported based on experimental and computational studies (Mazier et al. 2008; Spronk et al. 1999; Spronk et al. 1996).

Although other damages such as Met or His oxidations were predicted by a radiolytic attack simulation model (Gillard et al. 2007), our study clearly shows that the Tyr to DOPA modifications change the properties of the headpiece-DNA complex and thus may contribute to the destabilisation of the repressor-operator complex. Unfortunately, limiting our study to only a part of the repressor-operator system only allows us to provide a partial answer to the question of why irradiation abolishes repressor binding to DNA. As mentioned, allostery plays an important role in the binding of this protein to DNA. Binding of an effector (IPTG) to the core of the lactose repressor hinders its binding to DNA by triggering a global structural change of the protein including the modification of the positioning of the headpieces (Wilson et al. 2007). Therefore, it is possible that besides the modification of the oligomerisation state of the protein, damage to the core can affect DNA binding also via a global structural change (involving a change of headpiece position) by an allosteric effect. Moreover, the lack of the core in the simulation leads also to the freedom of the two headpieces with respect to each other. In reality they belong to a dimer stabilised by monomer-monomer interactions of the core regions. These strong interactions impose constraints on the positioning of the two headpieces. In the time span of our simulation, we did not observe significant relative displacement of the two headpieces, but this may occur at longer time scales. The fact that experimentally the affinity of a pair of linked headpieces (by an engineered Cys52-Cys52 bond) is much higher than that of the isolated headpiece and is similar to that of the tetrameric repressor (Kalodimos et al. 2004) suggests that hindering the movement of the isolated headpiece is necessary for complex stabilisation.

Protein damage is one of the multiple radiation-induced primary events that, under the influence of the cellular environment and after processing by cellular mechanisms, is involved in the deleterious effects of ionising radiation in vivo. Therefore, the results presented here give a new hint for understanding the mechanisms underlying these effects. Moreover, as similar protein damages result from other environmental oxidative stresses or even from age-related phenomena (Chakravarti and Chakravarti 2007; Davies and Dean 1997; Petropoulos and Friguet 2006), our results may also contribute to understanding molecular mechanisms involved in aging and stress-related pathologies.

Acknowledgments We gratefully acknowledge financial support from "La Ligue contre le cancer. Comité d'Eure-et-Loir (France)". The technical assistance of Alain Boyer is greatly appreciated.

References

Baker NA, Sept D, Joseph S, Holst MJ, McCammon JA (2001) Electrostatics of nanosystems: application to microtubules and the ribosome. Proc Natl Acad Sci USA 98:10037–10041

Begusova M, Spotheim-Maurizot M, Sy D, Michalik V, Charlier M (2001) RADACK, a stochastic simulation of hydroxyl radical attack to DNA. J Biomol Struct Dyn 19:141–158

Berman HM, Westbrook J, Feng Z, Gilliland G, Bhat TN, Weissig H, Shindyalov IN, Bourne PE (2000) The protein data bank. Nucleic Acids Res 28:235–242

Case DA, Pearlman DA, Caldwell JW, Cheatham TE III, Wang J, Ross WS, Simmerling CL, Darden TA, Merz KM, Stanton RV, Cheng AL, Vincent JJ, Crowley M, Tsui V, Gohlke H, Radmer RJ, Duan Y, Pitera J, Massova I, Seibel GL, Singh UC, Weiner PK, Kollman PA (2002) AMBER 9. University of California, San Francisco

Chakravarti B, Chakravarti DN (2007) Oxidative modification of proteins: age-related changes. Gerontology 53:128–139

Darden TA, York D, Pederson L (1993) Particle Mesh Ewald: an n log(n) method for Ewald sums in large systems. J Chem Phys 98:10089–10092

Davies MJ, Dean RT (1997) Radical-mediated protein oxidation. From chemistry to medicine. Oxford University Press, Oxford

Dolinsky TJ, Nielsen JE, McCammon JA, Baker NA (2004) PDB2PQR: an automated pipeline for the setup of Poisson-Boltzmann electrostatics calculations. Nucleic Acids Res 32(Web server issue):W665–W667

Dolinsky TJ, Czodrowski P, Li H, Nielsen JE, Jensen JH, Klebe G, Baker NA (2007) PDB2PQR: Expanding and upgrading automated preparation of biomolecular structures for molecular simulations. Nucleic Acids Res 35(Web Server issue):W522–W525

Eon S, Culard F, Sy D, Charlier M, Spotheim-Maurizot M (2001) Radiation disrupts protein-DNA complexes through damage to the protein. The lac repressor-operator system. Radiat Res 156:110–117

Gillard N, Goffinont S, Bure C, Davidkova M, Maurizot JC, Cadene M, Spotheim-Maurizot M (2007) Radiation-induced oxidative damage to the DNA-binding domain of the lactose repressor. Biochem J 403:463–472

Goffinont S, Davidkova M, Spotheim-Maurizot M (2009) Radiation-induced tetramer-to-dimer transition of *Escherichia coli* lactose repressor. Biochem Biophys Res Commun 386:300–304

Humphrey W, Dalke A, Schulten K (1996) VMD: visual molecular dynamics. J Mol Graph 14(33–8):27–28

Jain R, Freund HG, Budzinsky E, Sharma M (1997) Radiation-induced formation of 3,4-dihydroxyphenylalanine in tyrosine-containing peptides and proteins as a function of X-irradiation dose. Bioconjug Chem 8:173–178

Kalodimos CG, Boelens R, Kaptein R (2004) Toward an integrated model of protein-DNA recognition as inferred from NMR studies on the lac repressor system. Chem Rev 104:3567–3586

Klepeis JL, Lindorff-Larsen K, Dror RO, Shaw DE (2009) Long-timescale molecular dynamics simulations of protein structure and function. Curr Opin Struct Biol 19:120–127

Kollman PA, Massova I, Reyes C, Kuhn B, Huo S, Chong L, Lee M, Lee T, Duan Y, Wang W, Donini O, Cieplak P, Srinivasan J, Case DA, Cheatham TE 3rd (2000) Calculating structures and free energies of complex molecules: combining molecular mechanics and continuum models. Acc Chem Res 33:889–897

Lavery R, Sklenar H (1988) The definition of generalized helicoidal parameters and of axis curvature for irregular nucleic acids. J Biomol Struct Dyn 6:63–91

Mazier S, Villette S, Goffinont S, Renouard S, Maurizot JC, Genest D, Spotheim-Maurizot M (2008) Radiation damage to a DNA-binding protein. Combined circular dichroism and molecular dynamics simulation analysis. Radiat Res 170:604–612

Petropoulos I, Friguet B (2006) Maintenance of proteins and aging: the role of oxidized protein repair. Free Radic Res 40:1269–1276

Pettersen EF, Goddard TD, Huang CC, Couch GS, Greenblatt DM, Meng EC, Ferrin TE (2004) UCSF Chimeria-ar visualization system for exploratory research and analysis. J Comput Chem 25:1605–1612

Ryckaert JP, Ciccotti G, Berendsen HJC (1977) Numerical integration of Cartesian equations of motion of a system with constraints: molecular dynamics of n-alkanes. J Comput Phys 23:327–342

Spronk CA, Slijper M, van Boom JH, Kaptein R, Boelens R (1996) Formation of the hinge helix in the lac repressor is induced upon binding to the lac operator. Nat Struct Biol 3:916–919

Spronk CA, Bonvin AM, Radha PK, Melacini G, Boelens R, Kaptein R (1999) The solution structure of lac repressor headpiece 62 complexed to a symmetrical lac operator. Structure Fold Des 7:1483–1492

Srinivasan J, Cheatham TEI, Cieplak P, Kollman PA, Case DA (1998) Continuum solvent studies of the stability of DNA, RNA and phosphoramidate-DNA helices. J Am Chem Soc 120:9401–9409

Strahs D, Schlick T (2000) A-Tract bending: insights into experimental structures by computational models. J Mol Biol 301:643–663

Wilson CJ, Zhan H, Swint-Kruse L, Matthews KS (2007) The lactose repressor system: paradigms for regulation, allosteric behavior and protein folding. Cell Mol Life Sci 64:3–16